Acta Astronautica 73 (2012) 237–249

Contents lists available at SciVerse ScienceDirect

Acta Astronautica

journal homepage: www.elsevier.com/locate/actaastro

Applications of multi-body dynamical environments: The ARTEMIS transfer trajectory design ☆

David C. Folta [a,*], Mark Woodard [a], Kathleen Howell [b], Chris Patterson [b], Wayne Schlei [b]

[a] National Aeronautics and Space Administration (NASA)/Goddard Space Flight Center, Greenbelt, MD, United States
[b] Purdue University, West Lafayette, IN, United States

ARTICLE INFO

Article history:
Received 2 March 2011
Received in revised form
4 November 2011
Accepted 8 November 2011
Available online 23 December 2011

Keywords:
ARTEMIS
Manifolds
Libration
Lissajous
Multi-body
Optimization

ABSTRACT

The application of forces in multi-body dynamical environments to permit the transfer of spacecraft from Earth orbit to Sun–Earth weak stability regions and then return to the Earth–Moon libration (L_1 and L_2) orbits has been successfully accomplished for the first time. This demonstrated that transfer is a positive step in the realization of a design process that can be used to transfer spacecraft with minimal Delta-V expenditures. Initialized using gravity assists to overcome fuel constraints; the ARTEMIS trajectory design has successfully placed two spacecrafts into Earth–Moon libration orbits by means of these applications.

Published by Elsevier Ltd.

1. Introduction

The exploitation of multi-body dynamical environments to permit the transfer of spacecraft from Earth to Sun–Earth weak stability regions and then return to the Earth–Moon libration (L_1 and L_2) orbits have been successfully accomplished. This demonstrated transfer is a final step in the realization of a design process that can be used to transfer spacecraft with minimal Delta-Velocity (ΔV) expenditure. Initialized using gravity assists to overcome fuel constraints, the Acceleration Reconnection and Turbulence, and Electrodynamics of the Moon's Interaction with the Sun (ARTEMIS) mission design have successfully placed two spacecrafts into Earth–Moon libration orbits by means of this application of forces from multiple gravity fields.

Various design methods relying on multi-body dynamics were applied to achieve these transfers [1–13]. The individual arcs in different regimes in the original concept were not actually connected through any dynamical systems analysis. In operations the trajectory design used established optimization techniques whose success was enhanced by the insight from the dynamical structure afforded by the manifold behavior. This permitted investigation of the full region of possible trajectories to meet the final target in the Earth–Moon system and to meet ARTEMIS spacecraft maneuver constraints. In performing these analyses, one quickly finds locations in the Sun–Earth multi-body regions, which meet spacecraft constraints and identifies multiple (neighboring) manifolds. The number and types of trajectory arcs to be blended into a single design were unique for ARTEMIS and, thus, a unique combination of the theoretical structures that have been previously identified [5–7]. Generation of manifolds from dynamical information, optimization of forward numerically integrated states, and the selection of trajectory states near various manifold structures were combined to ensure the design was successfully given inherent modeling, navigation, and maneuver execution errors.

☆ This paper was presented during the 61st IAC in Prague.

* Corresponding author. Tel.: +1 301 286 6082; fax: +1 301 286 0369.
E-mail addresses: david.c.folta@nasa.gov (D.C. Folta), howell@purdue.edu (K. Howell).

0094-5765/$ - see front matter Published by Elsevier Ltd.
doi:10.1016/j.actaastro.2011.11.007

The ARTEMIS design involves two distinct Sun–Earth libration orbits (L_1 and L_2) transfers, one for each spacecraft, which demonstrates the potential in the application. The design incorporated lunar gravity assists (one of which used a double gravity assist with a 13-day interval between lunar encounters) to archive the correct energy and orbital orientation to place the vehicles on the appropriate transfer arc. Having placed the spacecraft such that it can exploit the flow direction consistent with a Lissajous trajectory manifold to attain the final Earth–Moon orbital conditions, operational support then focused on maintaining the desired manifold structure or switching to a nearby manifold, given navigation errors and mismodeled perturbations as the flow shifts from dynamically stable to unstable modes.

Along this transfer trajectory, several maneuvers were executed, each adjusting the trajectory slightly, each converging to the chosen target of an Earth–Moon libration orbit insertion location at the desired epoch. These designs are very sensitive to mismodeled perturbations and to maneuver errors. The contribution of this paper is to describe the methodology and offer an account of the ARTEMIS transfer design process within the context of the multi-body dynamical environment. It addresses lunar gravity assists, manifold generation, the optimization techniques as well as numerical solutions, sensitivity of the transfer, and the operational navigation solutions, and trajectory design implemented.

1.1. ARTEMIS mission

The ARTEMIS mission was approved in May 2008 by NASA's Heliophysics Senior Review panel as an extension to the Time History of Events and Macroscale Interactions during Substorms (THEMIS) mission [14–18]. THEMIS encompasses five spacecrafts in Earth orbit. The ARTEMIS mission involves moving the two spacecrafts in the outermost elliptical Earth orbits and, with lunar gravity assists, re-directing the spacecraft to both the L_1 and L_2 Earth–Moon libration point orbits via transfer trajectories that exploit both the Sun–Earth and Earth–Moon multi-body dynamical environments. The two spacecraft are denoted as P1 for the THEMIS B spacecraft and P2 for the THEMIS C spacecraft. The THEMIS team had long known that substantial orbit maneuvers would be necessary for both the P1 and P2 spacecraft to avoid entering a deep umbra shadow that would drain all power from the batteries and put the spacecraft into a non-recoverable power state. At the request of the Principal Investigator (PI), analysts at the Jet Propulsion Laboratory (JPL) designed transfer trajectories for both P1 and P2 to insert them into Earth-Moon libration point orbits [19]. The maneuver plan included a series a propulsive Orbit-Raising Maneuvers (ORMs) to position each spacecraft for a series of lunar and Earth gravity assist maneuvers. The injections into the translunar orbits for P1 and P2 occurred in January and March 2010.

As a final multi-body mission goal, ARTEMIS are the first spacecrafts to navigate to and perform stationkeeping operations around the Earth–Moon L_1 and L_2 Lagrangian points. The P1 spacecraft entered the Earth–Moon L_2 Lissajous orbit on August 25, 2010 and the P2 spacecraft followed on October 22, 2010 entering Earth-Moon L_1. On June 27th and July 17th of 2011, both spacecrafts were inserted into highly elliptical lunar orbits. ARTEMIS uses simultaneous measurements of particles and electric and magnetic fields from two locations to provide the first three-dimensional information on how energetic particle acceleration occurs near the Moon's orbit, in the distant magnetosphere, and in the solar wind. ARTEMIS has collected unprecedented observations of the refilling of the space environment behind the dark side of the Moon by the solar wind.

1.2. ARTEMIS partnership

The ARTEMIS mission is a collaborative effort between NASA's Goddard Space Flight Center's (GSFC) Navigation and Mission Design Branch (NMDB), the Jet Propulsion Laboratory (JPL) Mission Design and Navigation Section (MDNav), and the University of California at Berkeley (UCB) Space Sciences Laboratory (SSL). JPL provided the initial concept and the reference transfer trajectory from the elliptical orbit phase through libration orbit insertion and the details of the lunar orbit phase. GSFC's NMDB provided the operational trajectory design to complete the mission and the maneuver and navigation support from pre-lunar gravity assists and Sun–Earth transfers to Earth-Moon libration maintenance and lunar orbit insertion. The UCB SSL Mission Operations Center (MOC) provides spacecraft operations support (command, telemetry, maneuver planning, and daily monitoring and maintenance) of all spacecrafts. Tracking, telemetry, and command services are provided using the S-band frequency via various networks, including the Berkeley Ground Station (BGS), the Universal Space Network (USN), and the NASA Ground Network (GN) and Deep Space Network (DSN). UCB provides daily monitoring and maintenance of all spacecraft operations and the generation of maneuver commands for uploads using GSFC developed software.

1.3. ARTEMIS spacecraft overview

Each ARTEMIS spacecraft shown in Fig. 1 is approximately 0.95 m^2 per side panel and is spin-stabilized with a nominal spin rate of roughly 20 rpm. Spacecraft attitude and rate are determined using telemetry from a Sun sensor (SS), a three-axis magnetometer (TAM) used near Earth perigee, and two single-axis inertial rate units (IRUs). The propulsion system on each spacecraft is a simple monopropellant hydrazine blow-down system. The propellant is stored in two equally-sized tanks and either tank can supply propellant to any of the thrusters through a series of latch valves. Each observatory was launched with a dry mass of 77 kg and 49 kg of propellant, supplying a wet mass of 126 kg at the beginning of life.

Each spacecraft has four 4.4 N thrusters—two axial thrusters and two tangential thrusters. The two tangential thrusters are mounted on one side of the spacecraft and the two axial thrusters are mounted on the lower deck. The thrusters fire singly or in pairs – in continuous or

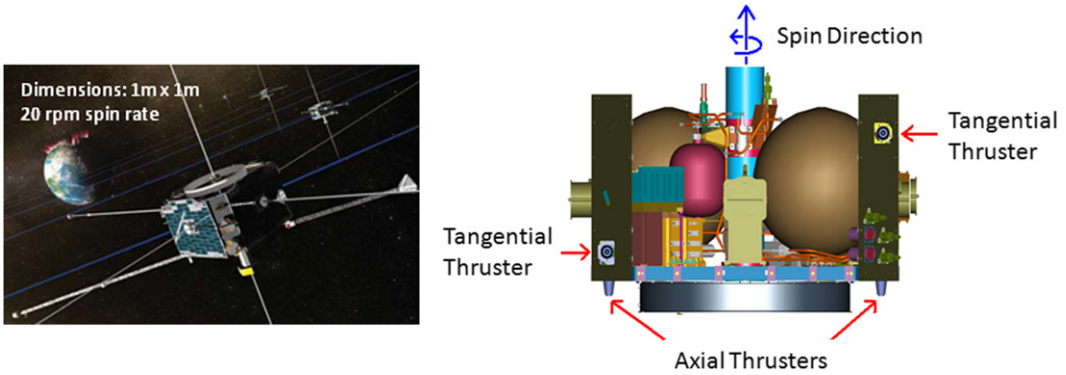

Fig. 1. ARTEMIS spacecraft and bus design. (For interpretation of the references to color in this figure, the reader is referred to the web version of this article.)

Table 1
ARTEMIS thruster firing modes.

Thurster firing modes			
Maneuver type	Thrusters involved	Depiction of operational mode	Purpose of maneuver
Axial thrust	A1 and A2 continuous firings		Perigee or apogee change or combined in-plane and out-of-plane orbit change with stowed EFI booms
Side thrust	T1 and T2 pulsed firing		Perigee or apogee change with deployed EFI booms
Beta thrust	A1 and A2 continuous firings alternating with T1 and T2 pulsed firings		In-plane and out-of-plane orbit change with deployed EFI booms
Attitude precession	A1 or A2 pulsed firing		Attitude change
Spin-up/spin-down	T1 or T2 continuous or pulsed firing		Spin rate adjustment

pulsed mode – to provide orbit, attitude, and spin rate control. Orbit maneuvers can be implemented by firing the axial thrusters in continuous mode, the tangential thrusters in pulsed mode, or a combination of the two (beta mode). Since there are no thrusters on the upper deck, the combined thrust vector is constrained to the lower hemisphere of the spacecraft. The propulsion system Isp was modeled at a constant 219 s.

1.4. ARTEMIS spacecraft maneuvers constraints

Each ARTEMIS probe's spin axis is pointed within 8° of the south ecliptic pole. These spacecraft can implement a Δv (thrust direction) along the spin axis towards the south ecliptic pole direction or in the spin plane, but cannot produce a Δv in the northern hemisphere relative to the ecliptic. While the axial thrusters were used when necessary, these thrusters are not calibrated as well as the tangential (radial) thrusters due to their infrequent use. The pointing constraint limited the location of maneuvers so most maneuvers were performed in a radial direction. For the lunar gravity assist and the multi-body dynamical environment, the trajectory was optimized using a nonlinear constraint that placed the Δv in the spin plane. The maneuver epoch was also varied to yield an optimal radial maneuver magnitude.

In addition to the direction of maneuvers, another 'error' source also resulted in some interesting maneuver planning. This is the fact that, as a spinning spacecraft, a maneuver will be quantized into Δv pulses of $\sim$1.5 cm/s each, with a start time that is dependent upon the Sun pulse in each spin. This meant that the achievable finite maneuver accuracy was dependent upon the Δv magnitude for each maneuver. Maneuvers were quantized by varying the maneuver epoch, but DSN coverage often led to this method not being easily enacted. Thus many early maneuvers were executed with the associated errors from spin pulse and timing. Later in the mission, the UCB operations team updated the onboard software to permit a variable spin-pulse to allow a more accurate match to the required Δv, reducing the uncertainty in the Δv per maneuver to less than 1%. Table 1 shows the ARTEMIS thruster firing modes.

2. Trajectory design

The ARTEMIS trajectory designs are illustrated in Figs. 2 and 3 [19]. The two diagrams show the ARTEMIS P1 and P2 trajectories in the Sun–Earth rotating frame during the

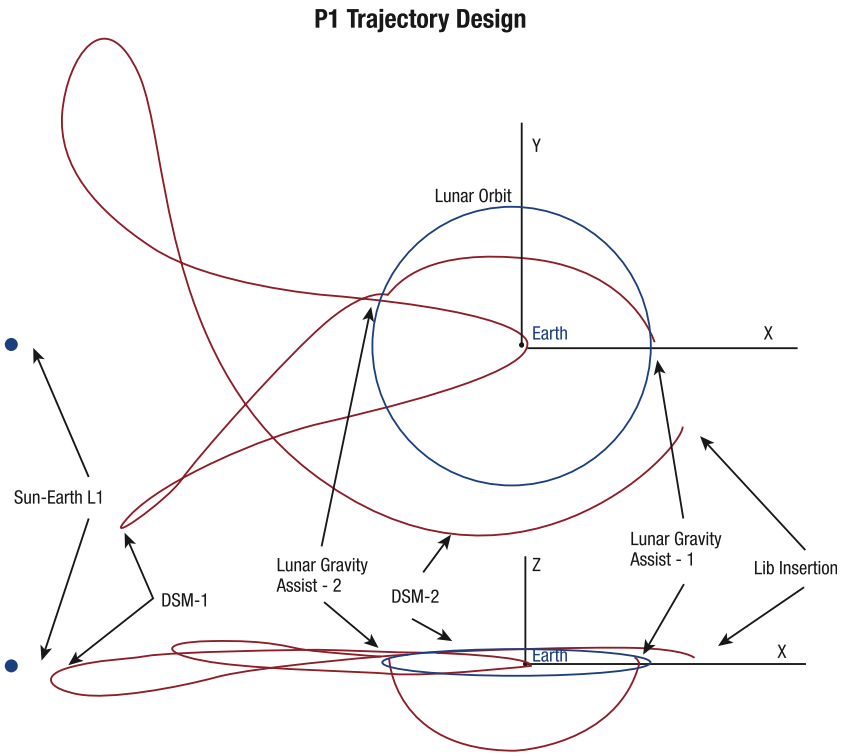

Fig. 2. ARTEMIS P1 trajectory design.

translunar phase. These general designs were originally determined using a dynamical process with a software tool called LTOOL [20,21]. During operations, this phase began with a carefully planned series of ORMs performed near periapsis to methodically raise apoapsis to lunar distance. The ORMs are carefully timed to phase the final apoapsis approach with lunar approach to achieve a lunar gravity assist maneuver. Gravity assists are a key component of the ARTEMIS trajectory design, as neither spacecraft has sufficient propellant to perform a direct insertion into the Earth–Moon libration point orbits. During the last few orbits prior to the lunar encounter, small Lunar Targeting Maneuvers (LTMs) and Trajectory Correction Maneuvers (TCMs) corrected for maneuver execution errors during the last ORMs and align the lunar approach trajectory to the proper B-plane targets.

2.1. Multi-body dynamical environment phase

Following the first close lunar gravity assist, the P1 spacecraft is placed on a southern ecliptic hemisphere transfer at roughly the lunar orbit radius and encounters a second gravity assist roughly 13 days later, as seen in the Sun–Earth rotating frame in Fig. 2. A Deep Space Maneuver (DSM1) was performed 33 days later. The DSM1 targets through Earth periapsis and to the Earth–Moon libration insertion state. Following the Earth periapsis, the P1 spacecraft once again transfers into the general vicinity of the Sun–Earth L_1 Lagrangian point. This region is also identified as a "weak stability boundary" region. At the final bend in the P1 trajectory, the spacecraft is at a maximum range of 1.50 million km from the Earth. At this point, the trajectory begins to fall back towards the Earth–Moon system. A Lissajous Insertion Orbit (LOI) maneuver was performed to insert P1 into the proper L_2 Lissajous orbit. The P2 translunar trajectory uses a single lunar swingby and three deep space maneuvers, two Earth periapses, and the Lissajous orbit insertion maneuver to insert P2 into the proper L_1 Lissajous orbit.

For both P1 and P2, 4% of the total propellant budget was allocated to perform any required TCMs along the way. The trajectory design focused on achieving the Earth–Moon libration insertion conditions to permit the final stage of the ARTEMIS mission, which includes a Lissajous orbit with a transfer to a high eccentric lunar orbit. Following the lunar flyby targeting phase that included several flybys at ranges from 50,000 km to just over 11,000 km, the transfer trajectory began. The flyby targets were required to enable the energy to place the ARTEMIS spacecraft near the appropriate outgoing manifolds. Since the two spacecraft were originally designed for a different mission, a highly elliptical Earth orbit, and were already flying, fuel was (and is) extremely limited. Thus, with the unique operational constraints, accomplishment of the transfer goals with the minimum cost in terms of fuel is the highest priority.

2.2. Perturbation model fidelity

A full ephemeris model (JPL's DE421 file) was used, which incorporated point mass gravity representing Earth, Moon, Sun, Jupiter, Saturn, Venus, and Mars. Also modeled

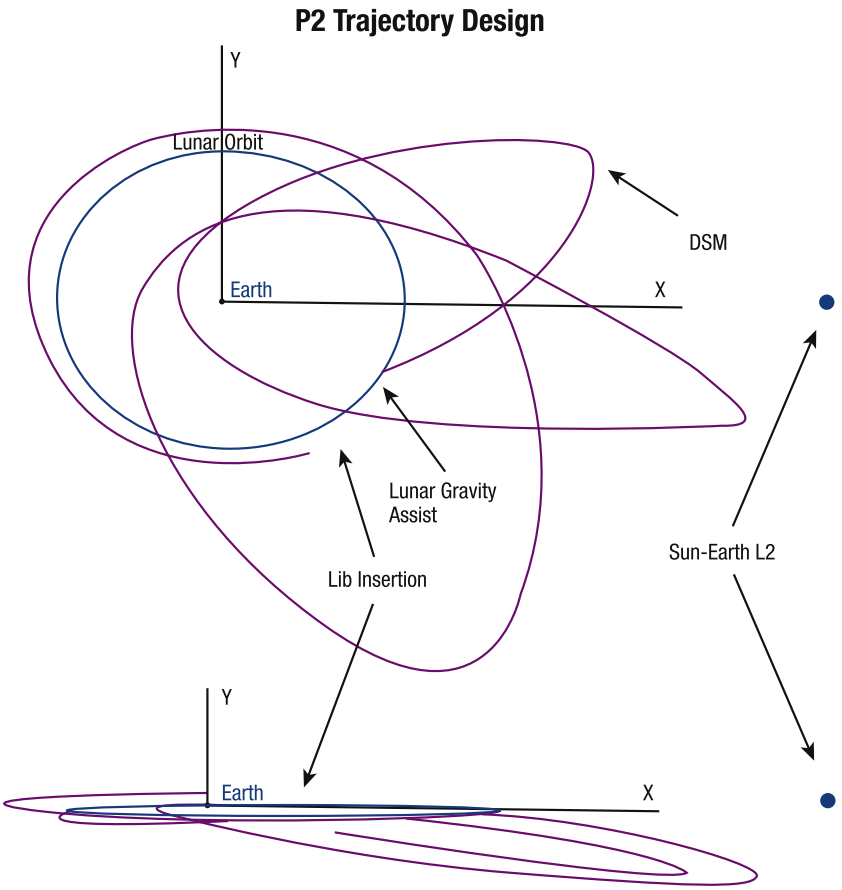

Fig. 3. ARTEMIS P2 trajectory design.

was an eighth degree and order Earth potential model. The solar radiation pressure force is based on the measured spacecraft area and the estimated mass (from bookkeeping) and the coefficient of reflectivity from navigation estimation. The trajectory simulations are based on a variable step Runge-Kutta 8/9 and Prince-Dormand 8/9 integrator. The libration point locations are also calculated instantaneously at the same integration interval. Initial conditions used throughout the maneuver planning process correspond to the UCB delivered navigation solutions using both the DSN and the UCB tracking system. While several coordinates systems are used, the ARTEMIS mission specified Earth Centered Cartesian (J2000) coordinates and an Earth–Moon rotating system were baselined. Software tools used in this process include the General Mission Analysis Tool (GMAT) developed at GSFC as an open source high fidelity tool with optimization and MATLAB® connectivity and AGI's STK/Astrogator suite.

2.3. Optimization of maneuvers

To compute maneuver requirements in terms of ΔV, our strategy involves various numerical methods: traditional Differential Corrections (DC) targeting with central or forward differencing and optimization using the VF13AD algorithm from the Harwell library [22]. A DC process provides for an a-priori condition and is also used for verification of the ΔV magnitude and direction. For the DC, equality constraints are incorporated, while for optimization, nonlinear equality and inequality constraints are employed. These constraints incorporate both the desired target conditions at the Earth–Moon system as well as the spacecraft constraints on the ΔV direction and relationship between the spin axis and the ΔV vector.

2.4. EM-libration insertion targets

The end goal of the transfer phase was to achieve the Earth–Moon Lissajous insertion conditions necessary for a minimal energy insertion into the Earth–Moon L_2 or L_1 Lissajous orbits. The goals were defined in terms of the Earth J2000 coordinates. These targets were held constant over the entire mission design process. As part of the early design process, a minimum ΔV was a constraint since the bulk of the fuel had been used in the prime Earth science mission. This left the designers with a fuel budget that could be used to raise apogee to reach the Moon directly, but without the required fuel to insert into lunar orbit. Although a baseline trajectory is defined to design the mission, there is no Earth–Moon L_2 or L_1 reference motion that is required. The only requirement is to attain a low

Table 2
Sample navigation solution uncertainties per phase during transfer trajectory.

Phase	Navigation arc length (days)	Position accuracy (m) (1σ)	Velocity accuracy (cm/s) (1σ)
P1 lunar assist 1	5	10	0.05
P1 lunar assist 2 (post FB)	2	1500	1.00
P1 deep space	21	34	0.09
P1 TCM2	7	43	0.11
P1 TCM5	7	43	0.11
Pre P1 Lissajous insertion	7	0.2	0.01
P2 lunar assist 1	3	30	0.01
P2 deep space	13	12	0.04
P2 TCM1	10	51	0.02
Pre P2 Lissajous insertion	7	0.7	0.05

lunar inclination once the spacecraft are transferred into elliptical lunar orbits.

2.5. Navigation uncertainties

Throughout the entire trajectory design process, navigation solutions were generated at a regular frequency of once every three days with the exception of post maneuver navigation solutions, which were made available once a converged solution was determined. The rapid response was to ensure that the maneuver had performed as predicted and that no unanticipated major changes to the design were necessary. Table 2 includes a list of the uncertainties of several navigation solutions used in maneuver planning. As seen, the RSS of the uncertainties are on the order of 10 s of meters in position and below 1 cm/s in velocity. As a conservative estimate for maneuver planning and error analysis, 1σ uncertainties of 1 km in position and 1 cm/s in velocity are used. These accuracies were obtained using nominal tracking arcs of one three-hour contact every other day. This frequency of contacts was investigated earlier in the mission design process and was thought to meet the accuracy goals as stated above. The Goddard Trajectory Determination System (GTDS) is used for all navigation estimation.

3. End-to-end trajectory design results

The original reference trajectory designs for the ARTEM/IS spacecraft were end-to-end solutions. However, in response to navigation, orbit determination and maneuver execution errors, and with a limited fuel budget, the trajectory response to errors and the maneuver options were further explored. Knowledge of the Sun–Earth/Moon dynamics was applied to verify that the target conditions would be met. Thus, the transfer trajectory design approach uses both the numerical methods as discussed above with the inclusion of dynamical systems analysis for verification and to gain insight into the transfer dynamics, which was incorporated for maneuver planning.

Recall that no requirement existed for the ARTEMIS spacecraft to remain near a reference path, rather the goal was simply to reach the target lunar orbit within the propellant budget. Thus, to design a maneuver, the spacecraft were first targeted to the libration point orbit insertion location knowing full well that maneuver execution and navigation errors would significantly alter the path. With a focus on the resulting delivery errors at the target location, a correction maneuver was planned that would essentially shift the trajectory. The trajectory shift at the maneuver point was determined such that the new path to the target condition would be consistent with a nearby manifold or the expected flow in this regime. An established method of calculating a manifold is the determination of the stable or unstable mode direction associated with a Sun–Earth or an Earth–Moon Lissajous trajectory via the monodromy matrix, and then using an off-set at an appropriate location along the Lissajous trajectory, integrating forward or backward along the stable or unstable direction. Lissajous orbits and manifolds can be approximated and computed in various models and has been accomplished by a number of authors [2,5,6,8–10,20,21,24,26,27]. Computing manifolds in the vicinity of the current trajectory is frequently the basic strategy employed to visualize the flow. An intersection of the resulting manifold with the 'current' trajectory can be used to identify a likely maneuver location and magnitude to yield a first guess in a targeting scheme.

While this approach has previously been successfully applied for maneuver planning, and was initially investigated as a means to determine a location for the maneuver in this analysis [30], an alternative strategy was selected to incorporate the spacecraft maneuver implementation constraints for the purpose of calculating optimized ΔVs. An optimization procedure permitted minimization of the ΔV magnitude, variation of the ΔV components in azimuth, as well as variation of the maneuver epoch, while incorporating the nonlinear constraint on the spacecraft ΔV direction relative to the spin axis. The manifold computations still supplied the intuitive design but could not be incorporated effectively as part of the algorithm at this point to also constrain the maneuver directions as required. Nevertheless, an example of two manifolds as applied to the ARTEMIS P1 trajectory design appears in Fig. 4. The left plot represents the computation of stable manifolds progressing towards a Sun–Earth L_1 Lissajous trajectory and illustrates (in red) a local manifold originating at the post-DSM position along the path and arriving in the vicinity of the Sun–Earth L_1 Lissajous orbit. The figure (right side) reflects unstable manifolds that depart from the Sun–Earth L_1 Lissajous trajectory, illustrating a local manifold (in red) that flows towards the point along this Sun–Earth unstable manifold that reaches the Earth–Moon L_2 Lissajous entry region, that is, it approaches the stable manifold associated with Earth–Moon L_2 Lissajous trajectory. The trajectory design reflects the merger of these two local manifolds to complete the mission (that is, the unstable manifold from the Sun–Earth L_1 region blends into the stable manifold that delivers the vehicle to the Earth–Moon L_2 vicinity). For flow information to serve as

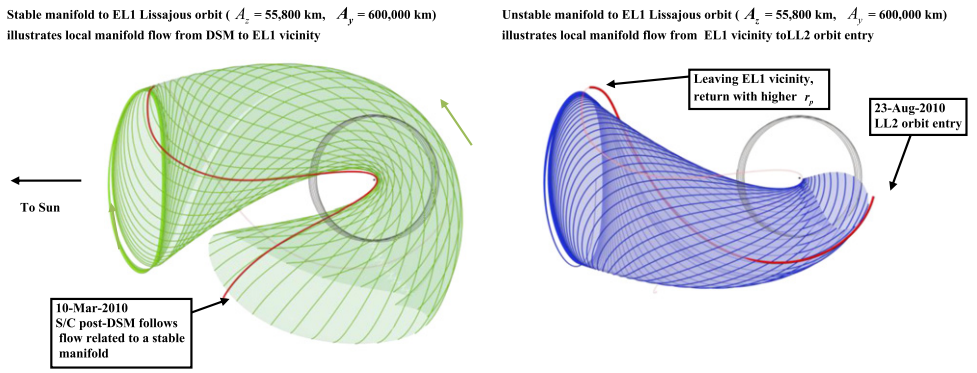

Fig. 4. Baseline P1 out-bound to max radius on stable manifold and in-bound to Lissajous orbit on unstable manifold.

a basis for the P2 transfer, the stable manifolds associated with the Earth–Moon L_2 Lissajous trajectory were propagated backwards and transformed directly to the Sun–Earth coordinate frame; the P2 path blended into the flow consistent the Earth–Moon manifolds directly from the relatively large DSM maneuver.

In reality, as the TCM maneuvers were performed, the path essentially jumped from the vicinity of one local manifold to another, at a slightly different energy level, to manage both the trajectory design requirements and the spacecraft constraints. The manifolds were generated using the initial condition (post-maneuver). To ensure that a verifiable trajectory solution was realized, the optimized maneuver solutions were correlated with these manifolds. In practice, with a focus on exploiting the natural flow when possible, the number of optimized maneuvers was very low and their magnitudes quite small, considering the sensitivity of the dynamics and uncertainties of the OD solutions.

3.1. Optimal ΔV maneuver design and placement

As the transfer trajectory was flown, correction maneuvers were required to adjust for maneuver execution errors as a result of the previous maneuver, the spacecraft pointing and implementation errors, as well as the navigation errors. These TCM maneuvers represent the statistical maneuvers along the transfer. A deterministic maneuver included in both P1 and P2 designs was called a Deep Space Maneuver (DSM), to separate it from maneuvers that were performed while in the elliptical orbit, which raised the aposapsis and eventually targeted the lunar gravity assists.

To target to the desired Earth–Moon Lissajous conditions, a VF13AD optimizer was used that incorporated the following variables and constraints. The representative ΔV control parameters for the correction maneuvers are maximum perturbations ranging from 1e-8 to 1e-10 and a maximum stepsize ranging from 1e-3 to 1e-5. These values can vary by a factor of ten, depending on the sensitivity of the trajectory. Table 3 lists sample P1 targeted states, epoch, and angle information wrt the spin axis. These targets where held constant throughout the transfer optimization.

Table 3
Sample linear and non-linear constraints.

S/C	Target/Constraint	Earth–Moon L2 goals (in Earth J2000 coordinate)	Tolerance
P1	*X* position	352,031 km	1 km
P1	*Y* position	−318,469 km	1 km
P1	*Z* position	−131,402 km	1 km
P1	Julian date epoch	24,55,431.500	60 s
P1	Non-linear: ΔV angle wrt Spin axis	89°	0.05°
P2	*X* position	353,345 km	1 km
P2	*Y* position	86,518 km	1 km
P2	*Z* position	71,174 km	1 km
P2	Julian date epoch	24,55,489.000	60 s
P2	Non-linear: Δv angle wrt Spin axis	89°	0.05°

Table 4
P1 trajectory correction maneuvers.

Maneuver	Epoch (UTCG)	ΔV magnitude (m/s)	Final maneuver error (%)	Reason for maneuver
DSM	March 10, 2010 @ 19:00	7.31	1.46	Deterministic ΔV
TCM 5	April 20, 2010 @ 09:00	0.18	−2.06	DSM correction
TCM 6	June 20, 2010 @ 21:45	0.18	−3.24	TCM 5 correction
TCM 7	July 19, 2010 @ 23:00	0.66	0.61	Arrival epoch
TCM 8	August 18, 2010 @ 06:00	2.24	n/a	Arrival epoch

At each maneuver location, the optimizer was run to determine the minimal ΔV location. To determine an a priori maneuver location and to achieve an intuitive "feel" for the maneuver results, a DC process was performed, which anticipated maneuver locations based on DSN coverage. Table 4 includes the P1 spacecraft maneuver

information for all the post-DSM transfer trajectory maneuvers. In Table 5, the P2 spacecraft maneuver information is listed for all the transfer trajectory maneuvers. Note that TCM numbers originate at '1', reflecting the corrections performed only in the multi-body dynamical environment phase. For P1, maneuvers TCM1 through TCM4 were completed in the elliptical orbit or during lunar gravity assist targeting. As shown in Tables 4 and 5, the maneuver execution errors are small at only a few percent. These errors are a function of actual start time wrt a sun pulse of a spinning spacecraft, tank temperatures, attitude knowledge, and the general propulsion system performance.

Figs. 5 and 6 show the major events, ΔVs, and locations of the P1 and P2 maneuvers during the multi-body dynamical environment phase in each case. The maneuvers compensate for the maneuver execution errors, the navigation errors, and the subsequent maneuvers to correct for these errors. These errors and small mismodeled perturbations can lead not only to late or early arrival times at the prescribe Lissajous insertion location, but also contribute to out-of-plane affects and may result in trajectories that intersect with the Moon. Clearly, the trajectory is very sensitive to such small perturbations. But, that sensitivity also implies that small corrections on the order of several cm/s can alter the trajectory design significantly and allow fine control.

The numerically generated trajectories for two maneuvers, the DSM and TCM5, appear in Fig. 7 as they were executed. Note how the resulting (post maneuver) trajectory varied due to maneuver execution and navigation errors as well as any mismodeling in solar radiation pressure. The largest difference is shown in the post-DSM trajectory as the maneuver error was significant at 11 cm/s. In the TCM5 maneuver used to correct the DSM error, the resultant accuracy yielded an error of 0.4 cm/s. This error was corrected in the TCM 6 maneuver. Two additional TCM maneuvers were then executed to adjust the arrival epoch into the Earth–Moon entry point and subsequent Lissajous trajectory. These time change maneuvers were required to permit the correct z amplitude-evolution in both the L_2 and

Table 5
P2 spacecraft maneuver information.

Maneuver	Epoch (UTC)	Δv magnitude (m/s)	Final maneuver error (%)	Reason for maneuver
TCM 1	March 26, 2010 @ 02:05	0.65	−0.60	Lunar flyby correction
DSM 1	May 13, 2010 @ 02:21	3.68	−3.43	Deterministic Δv
DSM 2	June 1, 2010 @ 14:50	23.30	−0.57	Deterministic Δv
TCM 2	July 20, 2010 @ 12:00	2.15	0.28	DSM 2 correction
TCM 3	August 2, 2010 @ 12:00	0.72	1.90	DSM 2 correction
DSM 3	September 9, 2010 14:00	3.28	n/a	Arrival epoch and EM L1 Z-evolution
TCM4	October 01, 2010 11:00	0.31	n/a	DSM 3 correction
TCM5	October 12, 2010 13:40	0.25	n/a	DSM 3 correction

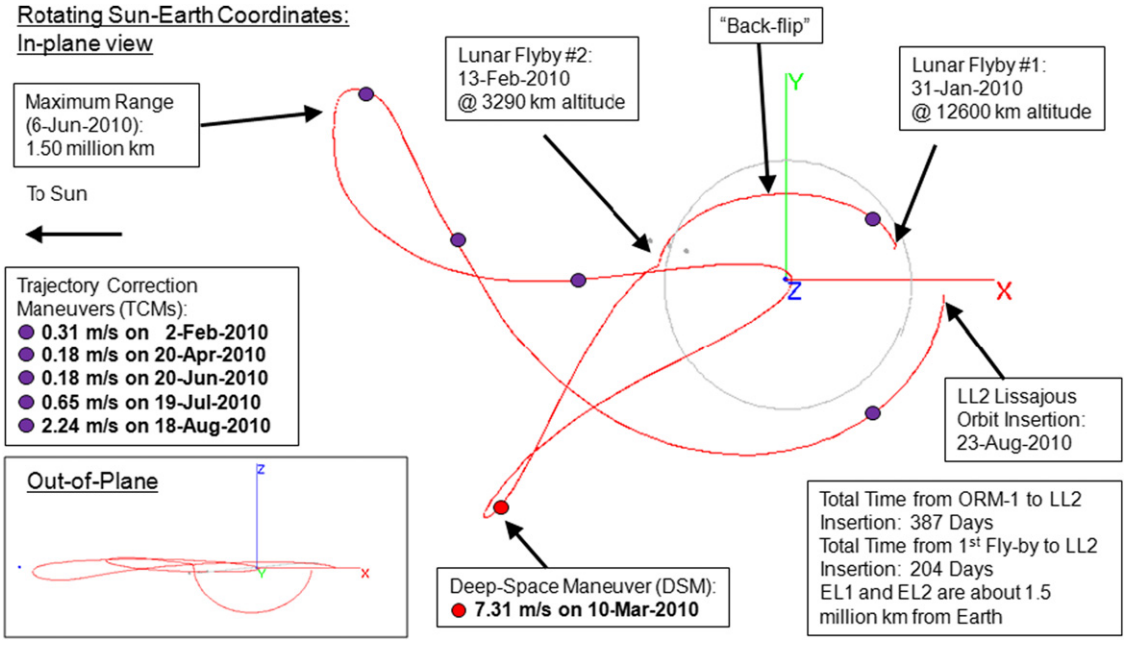

Fig. 5. P1 maneuver and major event locations.

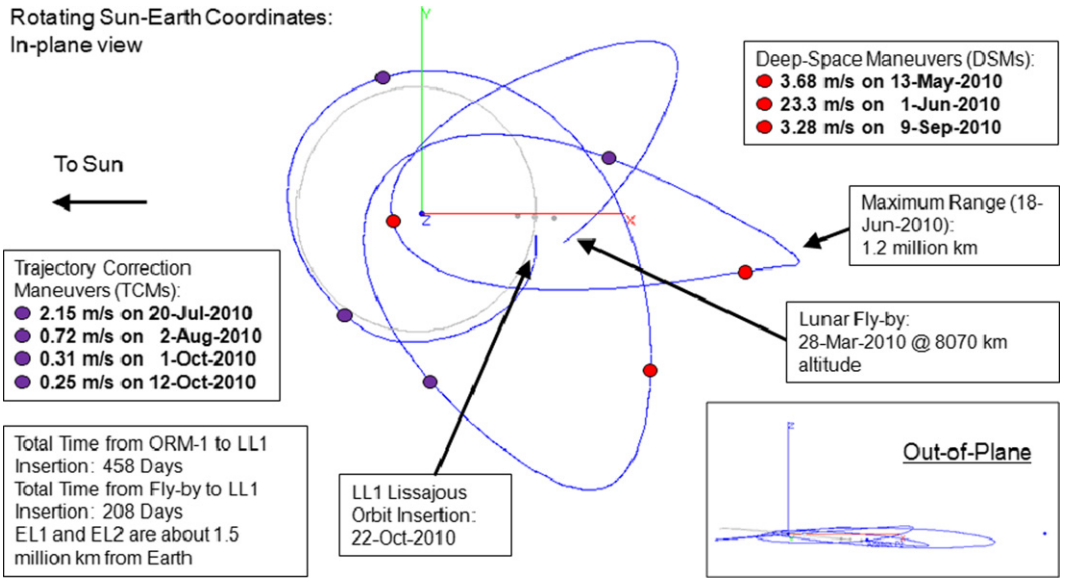

Fig. 6. P2 maneuver and major event locations.

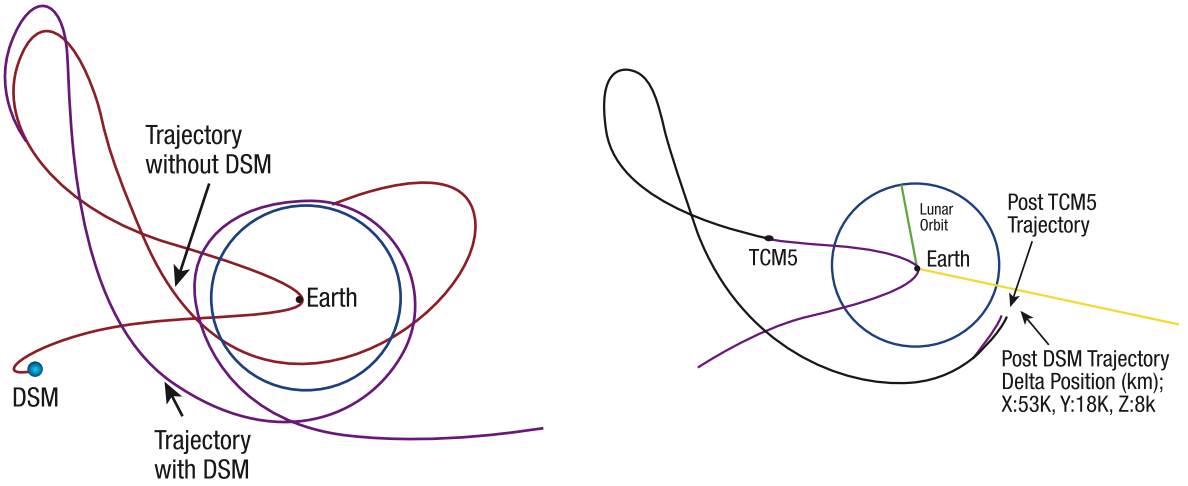

Fig. 7. Preplanning and optimized P1 DSM and post-DSM and optimized TCM5 trajectories.

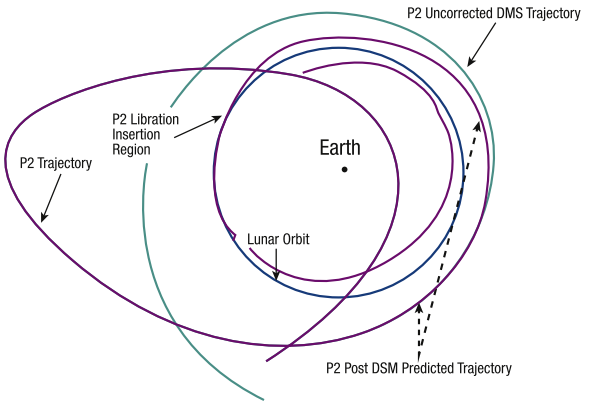

Fig. 8. Post P2 DSM and optimized TCM3 trajectories.

L_1 orbits. Recall that the z frequency is not correlated with the in-plane frequency, thus, a change to the Lissajous insertion time provides a method to adjust the initial velocities and Z component amplitudes. Fig. 8 presents the P2 trajectory for the optimized DSM and the correction TCM. As is apparent, the trajectory diverges after approximately one revolution around Earth, where the orbit radius is beyond the lunar orbit radius. In contrast, the corrected trajectory passes by the L_2 side using a half-Lissajous and then transfers to the Earth–Moon L_1 side.

4. Multi-body dynamical environment manifolds

Before discussing the flow in the multi-body dynamical environment that correlates with the ARTEMIS transfer path, a brief discussion of manifolds within this

context is offered [23–30]. In general, a stable or unstable manifold reflects the flow that asymptotically approaches or departs a fundamental solution such as a periodic orbit. For this application, a manifold is a representation of local trajectories that are subsequently numerically integrated in a full ephemeris model. Additionally, 'manifolds' are frequently represented either by the numerical results, by algorithms that define the state-space via lower-fidelity circular restricted modeling, or even by continuously differentially corrected arcs. The flow, in terms of the spacecraft states, is six-dimensional; for visualization, the manifolds are projected into configuration space and appear as two-dimensional surfaces in the circular restricted problem. The surfaces are approximated in higher fidelity models and yield very representative results for the flow. The manifolds plotted in this paper are constructed using initial states generated in an ephemeris model from the optimal or actual navigation solutions; these states are used to develop a Lissajous orbit for which the manifolds are produced. As a result, they represent a higher-fidelity model of all local (nearby) trajectories.

For ARTEMIS, manifolds that exist in the multi-body dynamical environment were generated to verify the numerically integrated, optimally planned, and actual post-maneuver results. The computation of manifolds also demonstrates the design process that can potentially shift a trajectory arc from the vicinity of one manifold to another and, thus, attain the targeted Lissajous insertion states (that is, an L_2 state for the P1 spacecraft and an L_1 state for the P1 spacecraft). These manifold computations are used essentially to interpret the effects of the DSM and the TCM maneuvers and to illustrate that the stable or unstable manifolds do, in fact, intersect near the maneuver locations. Manifolds are plotted for the pre- and post-DSM and TCM5 maneuvers of the P1 spacecraft and for the pre- and post-DSM trajectory arcs for the P2 spacecraft. In Fig. 9, the P1 stable manifold appears to reflect the actual trajectory as designed, for the optimal condition that would permit P1 to coast throughout the trajectory to the point of maximum excursion; subsequently, the spacecraft would closely follow the flow consistent with an unstable manifold to eventually arrive at the L_2 insertion location. But, as with all maneuvers and operations, errors in maneuver execution and navigation error affect the results.

4.1. Manifolds applied to the P1 spacecraft

As noted, for the P1 spacecraft, two manifolds are actually used to represent the behavior of the system, i.e., the stable manifold, which traverses the outbound trajectory and the unstable manifold, which provides a path to deliver the spacecraft to the Earth–Moon Lissajous orbit insertion state. But, for now, consider only the outbound arc and TCM5. From the DSM, P1 follows the original outbound path to the location of TCM5. Note that, if TCM 5 is to be implemented, the maneuver will shift the spacecraft to a different path, one that can be envisioned in terms of a different manifold. Subsequent to the DSM, and along the outbound trajectory, then, two outbound manifold arcs emerge from the TCM5 location and are plotted in Figs. 9, 10, and 12. These two manifolds represent the potential outcomes from (1) flow along the optimal path and (2) the alternative that incorporates a possible TCM5 maneuver. Fig. 9 presents the optimal (planned) DSM manifold. Note the location of the potential TCMs in this design. Fig. 10 reflects the maneuver effect of an exaggerated TCM5 applied to correct for a DSM execution error and demonstrates the P1 'jump' from the vicinity of one stable manifold (green) to an alternate transfer path that is represented by flow along another manifold (orange). An exaggerated view appears in Fig. 11 to highlight this manifold jump and visualize the shift in the flow directions that can result from a maneuver. For ARTEMIS, the manifolds were not directly incorporated to determine the optimal maneuver locations but to assess the feasibility and dynamical foundation of the overall structure of the design. Manifold intersections as part of the design process to determine maneuver locations can be done and has been proven both in research and in

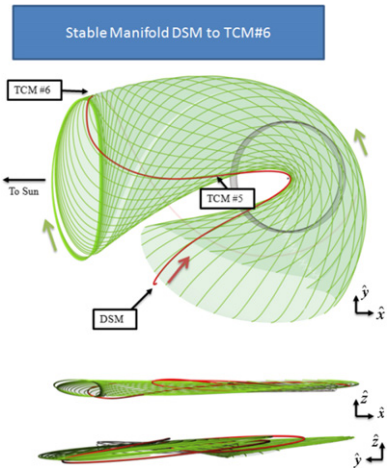

Fig. 9. P1 planned stable Sun–Earth manifold. (For interpretation of the references to color in this figure legend, the reader is referred to the web version of this article.)

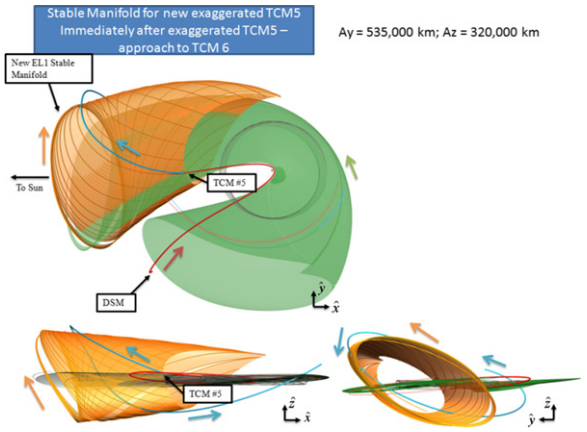

Fig. 10. P1 pre and post TCM5 stable Sun–Earth manifold. (For interpretation of the references to color in this figure legend, the reader is referred to the web version of this article.)

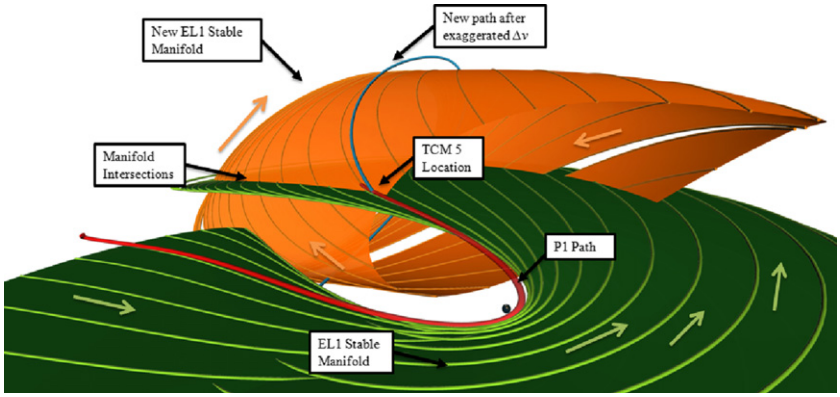

Fig. 11. Exaggerated post DSM and post TCM5 P1 stable manifolds. (For interpretation of the references to color in this figure legend, the reader is referred to the web version of this article.)

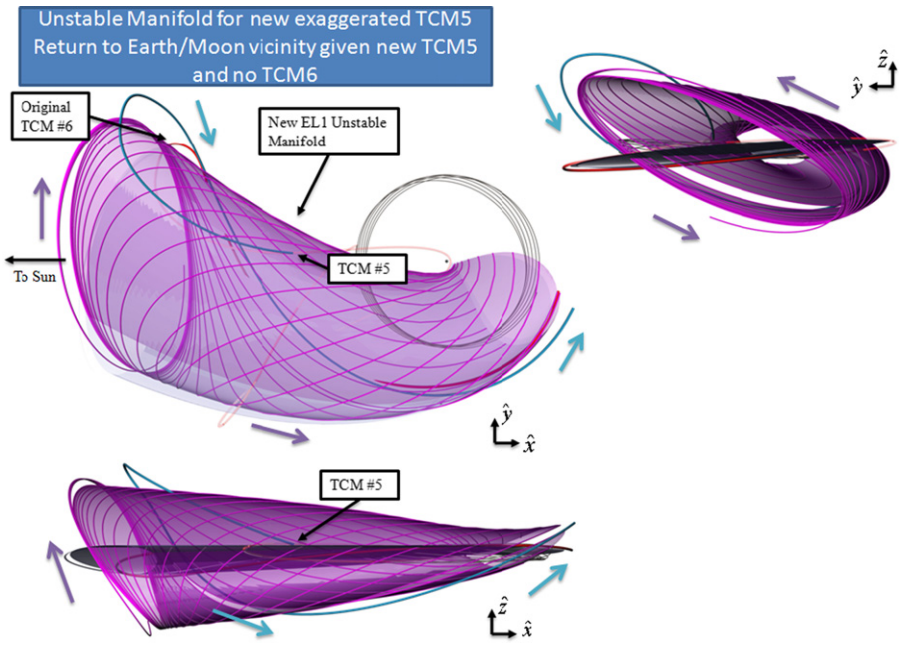

Fig. 12. P1 post TCM5 unstable manifold to L_2 Lissajous targeted state.

operations for the Genesis mission [31,32]. The P1 unstable manifold and the effect of TCM5 on the return portion of the orbit are plotted in Fig. 12 for an exaggerated TCM5 maneuver. The figure includes the original planned and the corrected post TCM5 trajectory. For the actual, relatively small TCM5 maneuver, the difference is slight in terms of the larger design but the shift in the general direction of the flow is consistent with a new manifold; the post TCM5 path with a small shift in direction guaranteed that P1 would reach its goal at the proper epoch.

4.2. Manifolds applied to the P2 spacecraft

The actual path for the P2 spacecraft (blue) as well as a computed manifold surface (green) appears in Fig. 13. This manifold design reflects the corrected manifolds to deliver the vehicle directly from the DSM to the vicinity of the Earth–Moon Lissajous stable manifold. Off-nominal conditions require a maneuver that shifts to the vicinity of this same manifold to successfully arrive at the Earth–Moon Lissajous orbit. Similar to the P1 design, the manifold is used to verify the feasibly of the optimized correction maneuver. The P2 spacecraft also jumps or shifts from the vicinity of one manifold to flow in a direction consistent with the required manifold at the maneuver location.

5. Discussion

The ARTEMIS mission provided many challenges and opportunities. The challenges of the spacecraft constraints, the multi-body dynamical environment, and the navigation performance can be overcome by the judicious use of optimization tools and manifold generation for verification.

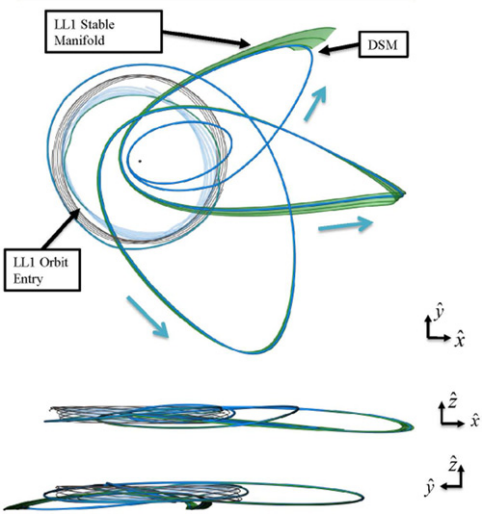

Fig. 13. P2 manifold. (For interpretation of the references to color in this figure legend, the reader is referred to the web version of this article.)

Several reliable software tools were available to permit cross checking of all maneuver plans and predicted trajectories. The overall sensitivity of the trajectory to the dynamical environment was found to be near the anticipated (pre-mission simulation analyses) ΔV control levels of cm/s as those proposed from many theoretical investigations and from recent operational missions that briefly flew trajectories, which passed thought these multi-body dynamical environments (WIND, SOHO, and WMAP for example). Small errors produced a large effect on the transfer design, but small, well-placed maneuvers can also correct these errors. While there are a number of strategies available that incorporate the Earth–Moon dynamics, the actual mission applications and mission constraints must also be considered. The methods developed here allow a general application whether there is a single target state, reference orbit, spacecraft constraints on ΔV direction, or orbital parameters requirements. The required transfer ΔV budget can be minimized by traditional targeting methods but the capability to reduce this budget to a very low level is substantially enhanced by exploiting the dynamical structure.

6. Conclusions

The ARTEMIS mission is an absolute success and this success can be attributed to the use of several tools to validate and confirm the planning and execution of maneuvers necessary to transit a dynamically challenging environment. The combined method of optimization with manifold verification, thought not new, is a substantial leap in the operational design of such missions. With the completion of the ARTEMIS trajectory, a viable multi-tiered process and trajectory feasibility is demonstrated. The opportunities of the ARTEMIS mission provide the space community with the first ever completed design from Earth elliptical orbit to the Earth–Moon L_2 and L_1 Lissajous orbits. Both ARTEMIS P1 and P2 spacecraft have completed their multi-body dynamical environment transfers and Earth–Moon L_2 Lissajous trajectories and are now in elliptical lunar orbits.

Acknowledgments

The authors would like to acknowledge Dan Cosgrove, Manfred Bester, Sabine Frey, Jeff Marchese, Brandon Owens, and all the operations personnel at the University of California, Berkeley. Their operational expertise and open communications ensured a successful mission. Also, we would like to thank our JPL colleagues; Steve Broschart, Ted Sweetser, and Greg Whiffen for their outstanding baseline concept and assistance in planning and executing the aforementioned maneuvers.

References

[1] D. Folta, F. Vaughn. A survey of Earth–Moon libration orbits: stationkeeping strategies and intra-orbit transfers, Paper no. IAC-02-Q.6.08, in: Proceedings of the 53rd International Astronautical Congress, World Space Congress, Houston, TX, USA, October 10–19, 2002.
[2] K.C. Howell, B.T. Barden, R.S. Wilson, M.W. Lo, Trajectory design using a dynamical systems approach with application to GENESIS, AAS/AIAA Astrodynamics 1997, Advances in the Astronautical Sciences, vol. 97, Part II, F. Hoots, B. Kaufman, P. Cefola, D. Spencer (Eds.), 1997, pp. 1665–1684.
[3] K.C. Howell, S.C. Gordon, Orbit determination error analysis and a station-keeping strategy for Sun –Earth L_1 libration point orbits, J. Astronaut. Sci. 42 (2) (1994) 207–228.
[4] G. Gómez, J. Llibre, R. Martínez, C. Simó, Dynamics and Mission Design Near Libration Points, I: Fundamentals: The Case of Collinear Libration Points, World Scientific Monograph Series, World Scientific Publishing Ltd., Singapore, 2001.
[5] W.S. Gómez, M.W. Koon, J.E. Lo, J. Marsden, Masdemont, S.D. Ross, Connecting orbits and invariant manifolds in the spatial restricted three-body problem, Nonlinearity 17 (2004) 1571–1606.
[6] F. Topputo, M. Vasile, F. Bernelli-Zazzera, Low energy interplanetary transfers exploiting invariant manifolds of the restricted three-body problem, J. Astronaut. Sci. 53 (4) (2005) 353–372.
[7] K.C. Howell, B.G. Marchand., Natural and non-natural spacecraft formations near the L_1 and L_2 libration points in the Sun–Earth/Moon ephemeris system, Dynamical Syst. 20 (1) (2005) 149–173 Special Issue: Dynamical Systems in Dynamical Astronomy and Space Mission Design.
[8] W.S. Koon, M.W. Lo, J.E. Marsden, S.D. Ross. 2000, Shoot the Moon, Spaceflight Mechanics 2000, AAS vol. 105, Part II, pp. 1017–1030.
[9] W.S. Koon, M.W. Lo, J.E. Marsden, S.D. Ross, Low energy transfer to the Moon, Celest. Mech. Dyn. Astr. 81 (2001) 63–73.
[10] J.S. Parker, G.H. Born, Modeling a low-energy ballistic lunar transfer using dynamical systems theory, J. Spacecraft Rockets 45 (6) (2008) 1269–1281 November–December.
[11] J.S. Parker, G.H. Born, Direct Lunar Halo Orbit Transfers, Paper AAS 07-229, in: Proceedings of the Seventeenth AAS/AIAA Space Flight Mechanics Conference, Sedona, Arizona, USA, January 28–February 1, 2007.
[12] C. Renault, D. Scheeres, Statistical analysis of control maneuvers in unstable orbital environments, J. Guid. Control Dynam. 26 (5) (2003) 758–769.
[13] R. Marson, M. Pontani, E. Perozzi, P. Teofilatto, Using space manifold dynamics to deploy a small satellite constellation around the Moon, Celest. Mech. Dyn. Astr. 106 (2) (2010) 117–142.
[14] M. Woodard, D. Folta, D. Woodfork, ARTEMIS: The first mission to the lunar libration points, in: Proceedings of the 21st International Symposium on Space Flight Dynamics, Toulouse, France, September 28–October 2, 2009.
[15] V. Angelopoulos, The THEMIS mission, Space Sci. Rev. 141 (2008) 5–34, doi:10.1007/s11214-008-9336-1.
[16] V. Angelopoulos, The ARTEMIS mission, Space Sci. Rev. doi:10.1007/s11214-010-9687-2.

[17] D.G. Sibeck, V. Angelopoulos, D.A Brain, G.T. Delory, J.P. Eastwood, W.M. Farrell, R.E. Grimm, J.S. Halekas, H. Hasegawa, P. Hellinger, K.K. Khurana, R.J Lillis, M. Øieroset, T.D. Phan, J. Raeder, C.T. Russell, D. Schriver, J.A. Slavin, P.M. Travnicek, J.M. Weygand, ARTEMIS science objectives and mission phases, Space Sci. Rev. doi:10.1007/s11214-011-9777-9 〈http://www.springerlink.com/content/p615274351124111/fulltext.pdf〉.
[18] M. Bester, M. Lesiw, B. Roberts, J. Thorsness, J. McDonald, D. Pease, S. Frey, D. Cosgrove, Multi-mission Flight Operations at UC Berkeley–Experiences and Lessons Learned, in: AIAA 2010, SpaceOps Conference Papers on Disk, Huntsville, AL, USA April 25–30, 2010, Paper AIAA-2010–2198.
[19] S.B. Broschart, M.K. Chung, S.J. Hatch, J.H. Ma, T.H. Sweetser, S.S. Weinstein-Weiss, V. Angelopoulos, Preliminary Trajectory Design for the Artemis Lunar MissionAAS 09-382, AAS/AIAA Astrodynamics Specialist Conference, August 9–13, 2009, Pittsburgh, Pennsylvania. A.V. Rao, T.A. Lovell, F.K. Chan, L.A. Cangahuala. (Eds.). In: Advances in the Astronautical Sciences, vol. 134 Univelt, Inc., San Diego, USA, 2009, AAS/AIAA.
[20] W.S. Koon, M.W. Lo, J.E. Marsden, S.D. Ross, Heteroclinic connections between periodic orbits and resonance transitions in celestial mechanics, Chaos 10 (2) (2000) 427–469.
[21] Lo, M., LTOOL Version 1.0 G Delivery Memorandum, JPL interoffice memorandum, September 20, 2000.
[22] Harwell Subroutine Library, Science and Technology Facilities Council, UK, 2011, 〈http://www.hsl.rl.ac.uk/archive/〉.
[23] G. Gómez, A. Jorba, J. Masdemont, C. Simó, Study of the transfer from the Earth to a halo orbit around the equilibrium point L_1, Celest. Mech. Dyn. Astr. 56 (4) (1993) 541–562.
[24] K.C. Howell, D.L. Mains, B.T. Barden, Transfer trajectories from earth parking orbits to Sun-Earth Halo orbits, AAS/AIAA Space Flight Mechanics Meeting 1994. In: Advances in the Astronautical Sciences, vol. 87, J. Cochran, C. Edwards, S. Hoffman, R. Holdaway (Eds.), 1994, pp. 399–422.
[25] B.T. Barden, K.C. Howell, Fundamental motions near collinear libration points and their transitions, J. Astronaut. Sci. 46 (4) (1998) 361–378.
[26] E.A. Belbruno, Sun-perturbed Earth-to-Moon transfers with ballistic capture, J. Guid. Control Dynam. 16 (4) (1993) 770–775.
[27] E.A. Belbruno. The Dynamical Mechanism of Ballistic Lunar Capture Transfers in the Four Body Problem from the Perspective of invariant Manifolds and Hill's Regions, Institut D'Estudis Catalans CRM Research report no.270.
[28] M. Bello-Mora, F. Graziani, P. Teofilatto, C. Circi, M. Porfilio, M. Hechler, A systematic analysis on weak stability boundary transfers to the moon, in: Proceedings of the 51st International Astronautical Congress IAF-00-A.6.03, Rio de Janeiro, Brazil, 2000.
[29] K.C. Howell, B.T. Barden, M.W. Lo, Application of dynamical systems theory to trajectory design for a libration point mission, J. Astronaut. Sci. 45 (2) (1997) 161–178.
[30] D.C. Folta, T.A. Pavlak, K.C. Howell, M.A. Woodard, D.W. Woodfork. Stationkeeping of Lissajous trajectories in the Earth-Moon System with applications to ARTEMIS, in: Proceedings of the Twentieth AAS/AIAA Space Flight Mechanics Meeting, San Diego, CA, USA, February 2010.
[31] B.T. Barden, R.S. Wilson, K.C. Howell, B.G. Marchand, Summer launch options for the genesis mission, in: AAS/AIAA Astrodynamics Specialists Conference, Quebec City, Canada, July 30–August 2, 2001.
[32] M. Lo, B. Williams, W. Bollman, D. Han, Y. Hahn, J. Bell, E. Hirst, R. Corwin, P. Hong, K. Howell, B. Barden, R. Wilson, GENESIS mission design, J. Astronaut. Sci. 49 (1) (2001) 169–184.